Liquid Crystals
Publication details, including instructions for authors and subscription information:
http://www.informaworld.com/smpp/title~content=t713926090

Flow patterns and disclination-density measurements in sheared nematic liquid crystals II: Tumbling 8CB

P. T. Mather[ab]; D. S. Pearson[a]; R. G. Larson[c]
[a] Department of Materials, University of California, Santa Barbara, CA, U.S.A. [b] USAF Phillips Laboratory, Edwards AFB, CA, U.S.A. [c] AT&T Bell Laboratories, Murray Hill, NJ, U.S.A.

To cite this Article Mather, P. T. , Pearson, D. S. and Larson, R. G.(1996) 'Flow patterns and disclination-density measurements in sheared nematic liquid crystals II: Tumbling 8CB', Liquid Crystals, 20: 5, 539 — 546
To link to this Article: DOI: 10.1080/02678299608031140
URL: http://dx.doi.org/10.1080/02678299608031140

LIQUID CRYSTALS, 1996, VOL. 20, NO. 5, 539–546

Flow patterns and disclination-density measurements in sheared nematic liquid crystals II: Tumbling 8CB

by P. T. MATHER*†§, D. S. PEARSON†¶, and R. G. LARSON‡

†Department of Materials, University of California, Santa Barbara CA 93106, U.S.A.

‡AT&T Bell Laboratories, Murray Hill, NJ 07974-0636, U.S.A.

(*Received 26 October 1995; accepted 14 November 1995*)

We examine the behaviour of nematic 4,4′-*n*-octylcyanobiphenyl (8CB) subjected to steady torsional shear flow at a temperature where this nematic is 'tumbling', i.e. the ratio α_3/α_2 of Leslie viscosities is negative. If the disc rotation speed is gradually increased from zero ($\dot{\theta} < 10^{-6}$ rad s^{-2}), the director eventually departs from the shear plane and becomes oriented radially. However, if the disc rotation speed is increased from rest at higher rates, twist wall defects are created sequentially at the sample meniscus and propagate inward with velocity $\approx 0{\cdot}85$ mm s^{-1}. Eventually, disclinations are nucleated. Disclination density measurements reveal that over similar ranges of values of the Ericksen number *Er*, samples of 8CB have roughly ten times the disclination density of the flow-aligning nematic, 5CB, reported in the preceding paper. Additionally, a transition from a power-law exponent of 0·5 to 1·0 for the dependence of dimensionless disclination density on *Er* is observed near $Er = 2000$, consistent with theoretical arguments.

1. Introduction

In the preceding paper of this two-part series [1], we reported measurements of disclination density during the shear flow of a flow-aligning nematic, 5CB. It was shown that despite the flow-aligning character of the material, disclinations are produced in significant quantities above a threshold shear rate. This supports previous observations of disclination formation in sheared flow-aligning samples of another flow-aligning nematic, MBBA [2, 3]. Given this surprising result—that flow-aligning nematics should produce disclinations at all—we now report directly comparable results for the tumbling nematic, 8CB, including the magnitude of disclination density observed during shear flow, the dependence of disclination density on shear rate, and the mechanism by which disclinations are formed. We will show that not only are disclination densities ten times higher than those reported for 5CB, but the mechanism of disclination formation is different as well. For a detailed review of the sequence of shear flow instabilities expected in tumbling nematics, we refer the reader elsewhere [4].

2. Experimental

8CB (4,4′-*n*-octylcyanobiphenyl) was purchased from EM Industries and used as received. Sample purity was confirmed by clearing transition measurements which showed agreement with literature values to within 0·1°C. 8CB has the phase sequence [5]: Cr 20·5°C S_A 33·3°C N 40·1°C CI. Except where noted, experiments were conducted at 37·0°C ($T_{NI} - T = 3{\cdot}1$°C).

The techniques described in the previous paper [1] are employed here, with the exception of the use of conoscopic observations to determine the out-of-plane rotation of the director and measurement of the width of the disclination density. The techniques of optical crystallography [6] can be easily applied to nematics because they have the same optical properties as uniaxial crystals.

To measure the width of the disclination density distribution, i.e. the thickness of the thinnest layer of the sample that contains almost all of the disclinations, a 20× objective lens is focused at positions finely spaced across the gap to detect the limiting positions between which some disclinations are in focus. This method is preferred over measuring the full distribution for cases where many measurements are required, such as determining the dependence of the distribution thickness on *Er*. When compared with disclination distribution measurements, $\rho_V(y)$ [1], λ is equivalent to the distribution width at a density 1/5 that of the distribution maximum.

For future use, we define the following quantities. $Er_R = (\gamma_1/K_3)\dot{\gamma}_R h^2$ is the Ericksen number at the edge (meniscus) of the sample cell, and is a function of the shear rate at the edge ($\dot{\gamma}_R$). Here, $\dot{\gamma}_R = \dot{\theta}R/h$, where $\dot{\theta}$ is the

*Author for correspondence.

§Current address: USAF Phillips Laboratory, OLAC PL/RKFE, Edwards AFB, CA 93524-7680, U.S.A.

¶Deceased.

0267-8292/96 $12·00

angular velocity of the rotating disc, and R is the radius of the cell. γ_1 and K_3 are, respectively, the twist viscosity, $\alpha_3 - \alpha_2$, and the Frank bend constant. We define Er (without subscript) to be the *local* value of the Ericksen number, which is calculated as $Er = (\gamma_1/K_3)\dot{\gamma}h^2$, where $\dot{\gamma} = r\dot{\theta}/h$ is the local shear rate at a radial distance r from the axis of rotation.

3. Results

3.1. *Qualitative observations*

We report the response of nematic 8CB in torsional shear flow for a wide range of rotation speeds and sample thicknesses, all at 37°C, where 8CB is a tumbling nematic; i.e. $\alpha_3 > 0$. We find that when 8CB is sheared, a variety of defect structures, or textures, occur, depending on the shear history of the sample. In particular, the texture depends not only on the rotation speed, but also on the rate at which the rotation speed is ramped from zero. As in the previous paper, we present here qualitative optical observations obtained using a variety of optical configurations in conjunction with our shear cell. Since the qualitative features depend upon the rate at which the rotation speed is increased; i.e. the angular acceleration of the rotating disc, the discussion below is divided into sections that each correspond to a different range of ramping rates.

3.1.1. *Low ramping rate*

When the ramping rate is very small, $< 10^{-6}$ rad s^{-2}, the director configuration in the cell undergoes a series of transitions which ultimately leads to the creation of large quantities of disclinations, much larger than are obtained in 5CB under these conditions. To observe the qualitative features of this regime, the time between fixed rotation speed increments ($\Delta\dot{\theta} = 10^{-4}$) must be larger than about 120 s. At low rotation speeds ($\dot{\theta} < 5 \times 10^{-3}$, $Er_R < 150$), the response of the initially homeotropic director is qualitatively the same as in 5CB, although the details of the pattern observed between crossed polarizers are dependent on the material parameters (α_i, K_i). In the photomicrograph shown in figure 1 (*a*), we see the director pattern at the cell centre when viewed through a 5× objective lens. The sample is between crossed polarizers and is illuminated with a He–Ne laser. As the rotation speed is increased from 5×10^{-4} (see figure 1 (*a*)) to 1×10^{-3} rad s^{-1} (see figure 1 (*b*)) the extinction ring spacing decreases due to the increasing gradient of director tipping.

As with 5CB, a further increase of the rotation speed leads to increasing fluctuations away from axisymmetry of the director pattern near the centre of the cell. The distortion of the pattern appears to be random in time and orientation. The degree to which these fluctuations

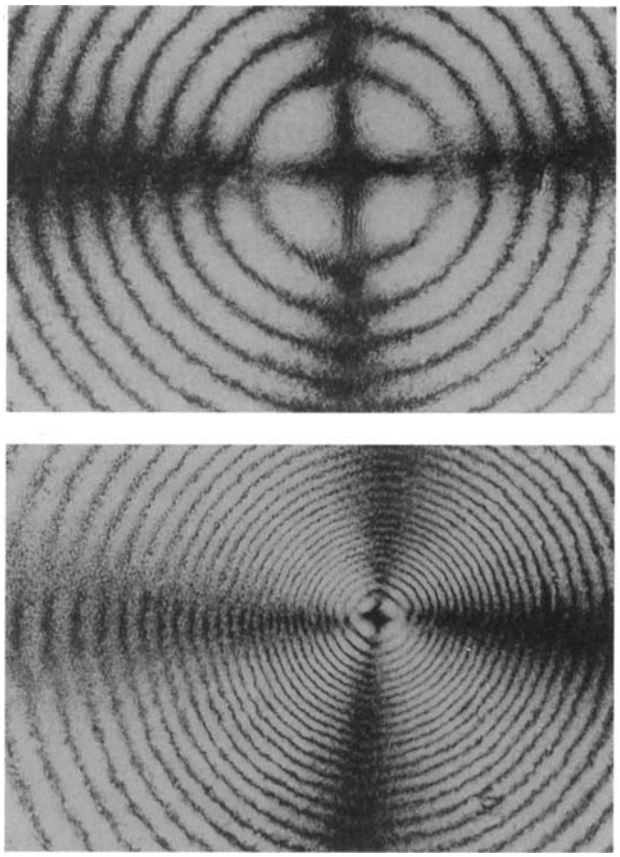

Figure 1. (*a*) Full view of 8CB between polarizers crossed at 0°/90° under He–Ne laser illumination ($\lambda = 632{\cdot}8$ nm). The sample thickness is 250 μm and the rotation speed is 5×10^{-4} rad s^{-1}. (*b*) The same at a speed of 1×10^{-3} rad s^{-1}. The field of view is 2 mm wide.

at the centre affect the director configuration in the cell as a whole is similar to that in 5CB; however, the base configuration is different in the two cases, as we will now discuss.

For the Ericksen number range $75 < Er < 200$, with Er referring to the *local* value of Er, we observe *bulk nucleation* of disclinations in 8CB. Figure 2 shows a representative photomicrograph of disclinations produced in this range of Er. In figure 2, disclinations are viewed with light polarized in the flow direction (vertical) and no analyser, and thin disclinations (*a*), monopoles (*b*), and thick disclinations (*c*) are observed in abundance. This texture is very similar to the threaded texture observed for all values of Er investigated ($Er < 5000$) in 5CB, with thicks and thins being equally numerous.

By increasing $\dot{\theta}$ in the slow ramping regime for various sample thicknesses (h) and observing the sample at various radial locations r, we find that the critical condition for this bulk nucleation phenomenon in controlled by the product $r\dot{\theta}h$, which shows that the critical condition is set

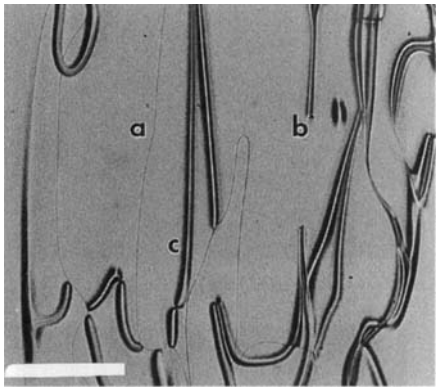

Figure 2. Photomicrograph of disclinations produced in 8CB in the range $75 < Er < 100$. The light is polarized in the flow direction (downward) and no analyser is in place. Shown are thin disclination lines (*a*), monopoles (*b*), and thick disclination lines (*c*). The reference bar is 450 μm in length.

by the local Ericksen number, Er. Increases in $\dot{\theta}$ beyond the value corresponding to $Er_R = 200$ lead to inward radial motion of the disclinations created over the range $75 < Er < 200$. The disclinations do not, however, penetrate the region near the axis of rotation, but are excluded from an interior zone whose outer boundary is defined by $Er = 75$. We refer to the zone containing disclinations as the 'disclination band'. Aside from the disclination band, the cell remains free of disclinations until a larger threshold Er is reached ($\gg 200$), at which disclinations fill almost the entire cell.

By observing the cell as a whole using 'full slit viewing' (see the previous paper [1]), with the laser light polarized at 45° with respect to the flow direction, and the analyser crossed with respect to the polarizer, we find that the formation of the disclination band initiates the departure of the director from the shearing plane for radii larger than that corresponding to $Er \approx 200$. (The shearing plane is locally defined as the plane containing both the flow direction and the flow-gradient direction.) The optical manifestation of an out-of-shearing-plane director configuration is that lines of equal transmitted light intensity are no longer closed, but instead form spirals, and the portion of the extinction rings viewed in the radial slit appear oriented at an angle with respect to the flow direction. This feature is shown in figure 3, where the sample is viewed between crossed polarizers oriented at 45° and 135° with respect to the flow direction near the edge (see figure 3 (*a*)) and with the full-slit view (see figure 3 (*b*)). The existence of an out-of-plane tipping of the director is confirmed by conoscopic observations which show near-planar conoscopic patterns rotated away from the shearing plane. For radii greater than the position where $Er = 200$, conoscopic patterns indicate that the director takes on a significant component of radial orientation, while for radii corresponding to $Er < 75$, the director remains confined to the plane of shear. Conoscopic patterns are not observed for $75 < Er < 200$ due to the presence of disclinations. For $Er > 800$, the director is nearly parallel to the vorticity direction; i.e. perpendicular to the shearing plane, for radii approximately 0·5 mm from the edge. These observations are summarized schematically in figure 4 in which the director orientations along a radius are represented by sticks, with a nail-head representing orientation into the page.

If the cell is viewed from above, with the bottom disc rotating *counter-clockwise*, the director rotates out of the shear plane for increasing Er or, equivalently, increasing radial position, with a *clockwise* sense. This is the same sense as the rotation that fluid particles experience due to the streamline curvature present in this flow geometry. In rectilinear shear flow, the direction of director rotation upon departing the shear plane is symmetric about the shear plane; i.e. the director feels an equal tendency to rotate clockwise as it does to rotate counter-clockwise. In torsional shear flow, however, the symmetry is broken by the streamline curvature.

At large enough angular velocities, *roll cells* are visible—though not appearing first at the edge. Roll cells are vortices parallel to the flow direction created by a secondary flow that is periodic in the vorticity direction. In shearing flow, tumbling nematics become unstable at high Er to roll-cell formation when the director is in the vorticity direction. [4, 7, 8] Our observations show that the critical value of Er for roll-cell formation is approximately 1000, which is in agreement with theoretical predictions [9], and with the critical value observed in a lyotropic polymer nematic, poly(γ-benzyl-glutamate). At this critical point, the roll cell pattern is weak, as shown in figure 5 (*a*) for $Er = 1000$, and intermittently appears and disappears. The roll cells increase their contrast and decrease their spacing as Er is further increased, eventually leading to prolific nucleation of disclination lines ($|S| = 1$) within the roll cell structure as shown in figure 5 (*b*) for $Er \approx 2000$. For both photomicrographs in figure 5, the sample is illuminated with light polarized in the flow direction—a condition required for the visualization of the roll cells—and viewed with no analyser. The disclinations that form have appearance similar to 'thicks', and form in the dark regions separating adjacent roll cells. Once they form, the disclinations increase their length rapidly (for example, from 50 to 500 μm) in approximately 100 ms. The formation process begins with a diffuse 'distortion' appearing between roll cells that suddenly sharpens, while simultaneously extending rapidly in the flow direction. Similar observations have been reported for the polymeric nematic, PBG, in plane Couette flow [4].

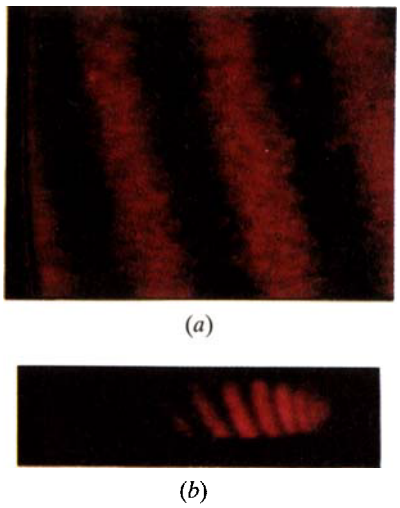

(*a*)

(*b*)

Figure 3. Orthoscopic images of 8CB sheared at $\dot{\theta}=0{\cdot}025$ rad s^{-1} ($h=300\,\mu$m) yielding Er greater than 100 for almost entire cell. (*a*) Magnified view, in which the field of view is 1·8 mm; (*b*) full-slit view with a slit width (vertical dimension) of 3·8 mm. The sample is illuminated with laser light ($\lambda=632{\cdot}8$ nm) polarized at an angle 45° to the flow direction and viewed with an analyser crossed with respect to the polarizer. Under these flow conditions the director begins to depart from the plane of shear, and the full view shows that the extinction lines are not parallel with the streamlines.

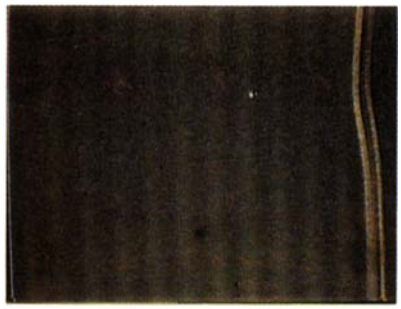

(*a*)

(*b*)

Figure 5. Observation of roll cells observed during shear flow of 8CB for $r=13$ mm, $h=300\,\mu$m and (*a*) $\dot{\theta}=0{\cdot}053$ rad s^{-1} ($Er\approx1000$) and (*b*) $\dot{\theta}=0{\cdot}1$ rad s^{-1} ($Er\approx2000$), in which thick lines nucleated from the sharpened roll cells. The field of view in each photomicrograph is 2 mm wide.

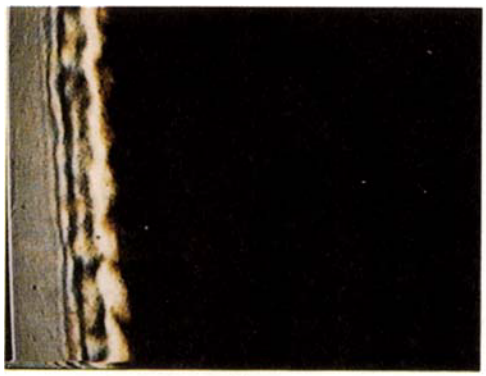

(*a*)

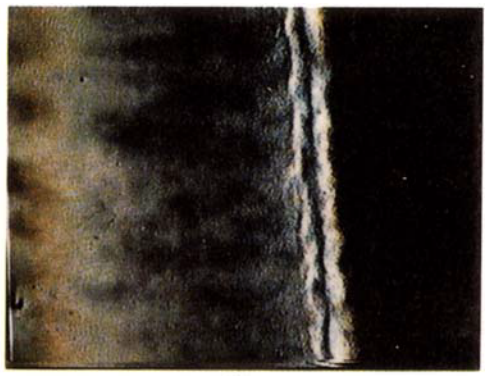

(*b*)

(*c*)

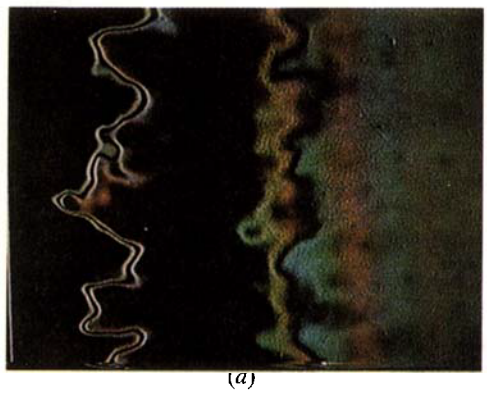

(*d*)

Figure 7. Radial propagation of a birefringent line (twist wall) which originated at the cell edge and moved toward the cell centre with a velocity of 0·85 mm s^{-1}. The sample is 8CB at 36·1°C, 225 μm thick, viewed near the cell edge, and the rotation speed is 0·03 rad s^{-1}. Photomicrographs were taken at times (*a*) 2, (*b*) 3, (*c*) 4, and (*d*) 5 s following shear start-up. The field of view in each photomicrograph is 2 mm wide, and the polarizer is oriented in the flow direction with the analyser crossed with respect to the polarizer.

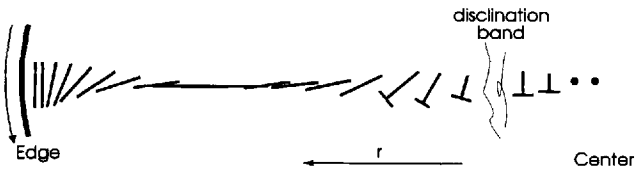

Figure 4. Schematic radial dependence of 8CB director orientation in which the director twists out of the plane of shear. The nail head represent orientation into the page.

In 8CB, roll cells and roll-cell nucleated disclinations coexist over only a small range of Er, above which the roll cell structure is obscured or eliminated by the large density of disclination lines. At the highest angular velocities studied, the texture is transformed to a 'chaotic' state of motion of scintillating small domains, here called the 'worm texture' after the nomenclature of Graziano and Mackley [3]. Observations of H_V light scattering [10] from this texture show large anisotropy with very gradual decay of scattered intensity with increasing scattering vector, $\mathbf{q}$, in the vorticity direction, the direction perpendicular to both the flow and flow gradient directions. This suggests that the texture (now defined in terms of domains, rather than disclinations) consists of anisotropic domains oriented in the flow direction. The worm texture is shown in figure 6 (*a*) and its associated scattering pattern is shown in the inset. This type of scattering pattern has also been observed for both thermotropic [11] and lyotropic [12] liquid crystalline polymers in shear flow. Shown in figure 6 (*b*) is the texture observed 1 min after cessation of flow, demonstrating the rapid coarsening of the worm texture toward the aligned state.

3.1.2. *Higher ramping rate*

If the acceleration of bottom disc from rest is larger, $\sim 3 \times 10^{-6}$ rad s^{-2}, disclinations fill the cell continuously above the same critical Er required to produce the disclination-band at the low ramping rate, namely $Er \sim 75$. In contrast to the previous case, however, when $Er = 200$ the disclination band does not disappear. Instead a further increase in Er leads to continued disclination creation, with the disclinations having the same appearance as those in the disclination band. A further increase in Er leads eventually to the creation of patches of roll cells at Er values similar to those required for them to form in the *low ramping rate* case. Superimposed on the roll cells is a high disclination-density threaded texture. In regions where roll cells appear superimposed on the disclinations, the density of disclinations is much smaller than in the surrounding regions. Thus, the director pattern present in roll cells is not completely compatible with that produced by disclinations. This is not surprising. Indeed, it is surprising that roll cells appear at all under these conditions, since one might think the presence of a large number of disclination lines would disable the establishment of the director configuration required for the onset of roll cells. At the highest Er values, the worm texture appears. Indeed, the appearance of the worm texture at high Er is a property of 8CB independent of the rate at which Er is ramped.

3.1.3. *Abrupt start-up*

If the angular velocity of the bottom disc is started from rest at a 'large' value ($\dot{\theta} > 0{\cdot}025$ rad s^{-1}, $Er_R > 1500$) a progression of highly birefringent lines oriented in the flow direction propagate inward from the edge. We call

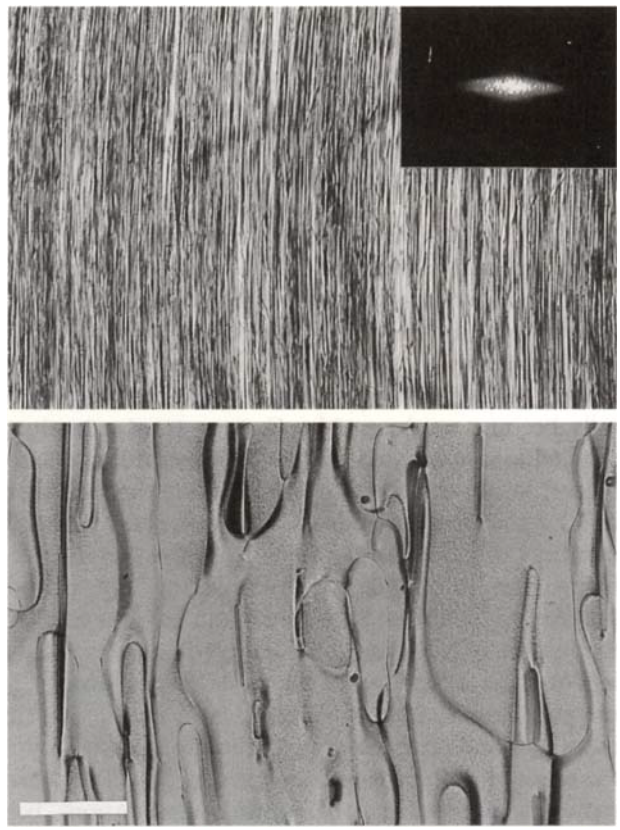

Figure 6. Photomicrographs showing disclinations formed in 8CB; (*a*) during steady shearing and (*b*) 1 min following shear cessation. The sample thickness is 300 μm, the disc rotation speed is 0·6 rad s^{-1}, and the viewing radius is 17 mm from the cell centre ($Er \cong 2 \times 10^5$). The sample is illuminated with light polarized in the flow (vertical) direction, and viewed with a 20× objective lens with no analyser present. The reference bar in the lower left portion of (*b*) corresponds to 500 μm. Inset in (*a*) is the H_V light scattering pattern observed for the same flow conditions using a He-Ne ($\lambda = 632{\cdot}8$ nm) laser polarized in the flow direction and viewed on an opaque screen above the sample and following passage through an analyser crossed with the polarizer. The width of the inset photograph corresponds to approximately 30°.

these defects 'twist walls', following the nomenclature of Carlsson and Skarp [13], who saw defects resembling the birefringent lines under similar conditions. It is likely that the twist walls result from sequential in-plane tumbling instabilities, in accord with the interpretation provided in [13].

In figures 7(*a*)-(*d*), photomicrographs taken from video tape show this interesting defect propagation, where defects move radially inward (left to right), with the first image taken 8·5 s after shear start-up, and with a 1 s time difference between each image. The propagation velocity for the outermost twist wall was measured to be $0{\cdot}85 \pm 0{\cdot}05\,\mathrm{mm\,s^{-1}}$, and was observed to increase with rotation speed (or Er_R). These observations may have bearing on the interpretation of the rheological observations on 8CB, as measured by Gu and Jamieson [14], in which the oscillatory shear stress response following shear start-up in a cone-plate rotational rheometer was progressively damped until no oscillations were visible after approximately 100 strain units. This will be the topic of a forthcoming paper [15].

3.2. *Disclination density measurements*

We reported above that 8CB forms roll cells above a critical Ericksen number and that disclinations are nucleated from this roll-cell structure. At a fixed Ericksen number above the threshold for roll-cell formation, the density of disclinations increases with time until the roll cells become unobservable. Once a steady density of disclinations is reached, *Er* can be increased, and a new, higher, steady-state density of disclinations establishes itself. As with 5CB, if *Er* is then decreased significant numbers of disclinations remain even when *Er* drops below the threshold observed during the previous (increasing *Er*) ramp. Shown in figure 8 is an example of the hysteretic behaviour of disclination density; here ρ_A is plotted as a function of *Er* for a 400 μm sample. The ramping rate, $\ddot{\theta}$, is approximately $10^{-6}\,\mathrm{rad\,s^{-2}}$. A large overshoot and undershoot in disclination density follows the onset off disclination formation at $Er \approx 2000$. Disclination form locally, at first, with disclinations being created in large quantities within a narrow range 1–2 mm wide of radial positions near the cell edge. As *Er* is further increased, the region of localized disclinations suddenly spreads out to encompass most of the cell. After this, the disclination density suddenly drops significantly, producing the undershoot shown in figure 8. After a further increase in *Er*, and the passage of time, the measured disclination density returns to the steady state curve subsequently measured for decreasing *Er*, shown as open symbols in figure 8. The exact shape of the curve for increasing *Er* depends on the ramping rate; qualitatively, we found that the overshoot and undershoot amplitudes decrease with decreasing ramping rate.

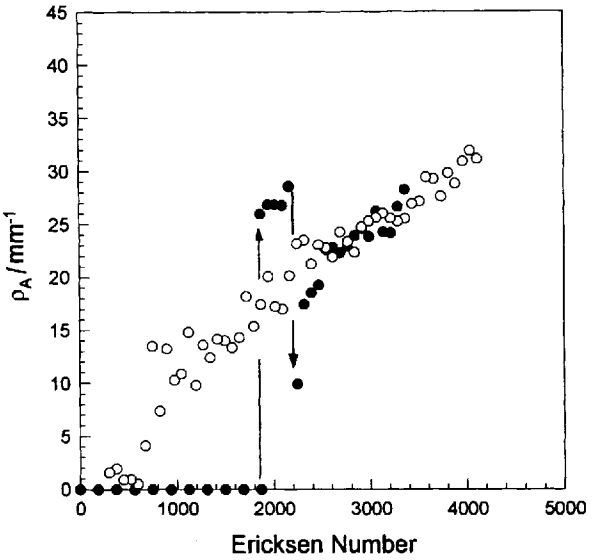

Figure 8. Disclination density, ρ_A, versus *Er* for increasing *Er* (filled symbols) and decreasing *Er* (open symbols) using *Er* ramping rates of $0{\cdot}1\,\mathrm{s^{-1}}$ and $-0{\cdot}1\,\mathrm{s^{-1}}$, respectively. Near $Er = 2000$, ρ_A suddenly jumps to large values. The details of the overshoot and undershoot during increasing *Er* are dependent on the ramping rate.

Using the 20× objective lens, the distribution of disclinations across the gap in the shear flow geometry is observed to be non-uniform, with the density being largest at the sample midplane and negligible at the glass surfaces. The distribution was measured for two sample thicknesses, $h = 200$ and 300 μm, for $Er = 2400$, and the results are plotted in figure 9. When plotted as the volumetric disclination density, ρ_V, normalized by the maximum value of ρ_V, the two distributions superpose well, and are similar to that of 5CB ([1], figure 9). Clearly, disclinations are repelled from the aligning surfaces, leading to a narrow Gaussian distribution centred at the sample midplane.

For 8CB, as with 5CB, plots of disclination density, ρ_A, versus applied shear rate, $\dot{\gamma}$, depend on the sample thickness. Data from various thicknesses and radial positions superpose when plotted as $\rho_A h$ versus *Er*, *indicating a lack of explicit dependence of disclination density on the radial position*. Recall that for 5CB, such plots did not superpose; plots of $\rho_A h$ versus *Er* differed from one radial position to the next. Figure 10 shows a plot of dimensionless disclination density, $\rho_A h$ versus *Er* for several gap thicknesses along with 5CB data for the large $\tilde{r}$ limit. The most striking feature of this plot is the contrast in magnitude of disclination density between the two materials—*the density of disclinations in 8CB is an order-of-magnitude higher than in 5CB.*

For all thicknesses studied, with the exception of the smallest, 250 μm, we find a cross-over in the exponent of

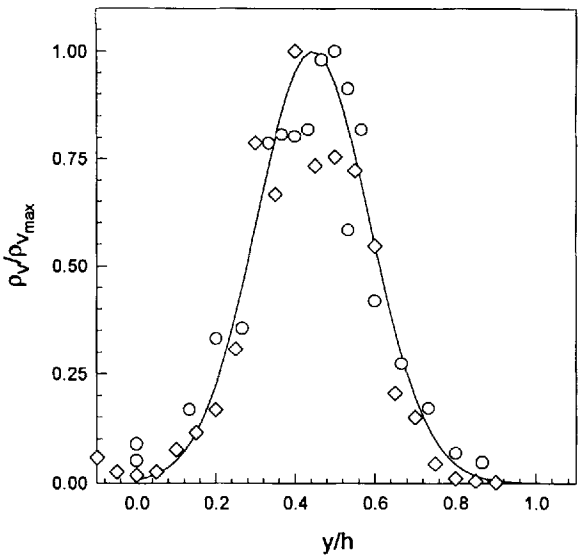

Figure 9. Profile of disclination density in 8CB for $h=200$ (◇) and 300 (○) μm at $Er=2400$, showing exclusion of disclinations from the boundaries. The profiles were measured using a 20× objective lens with a narrow (4 ± 1 μm) depth of focus. The volumetric disclination density (ρ_V) is scaled by the maximum value of the distribution, while the gap position (y) is scaled by the gap thickness. The solid line represents a Gaussian fit to the 300 μm data.

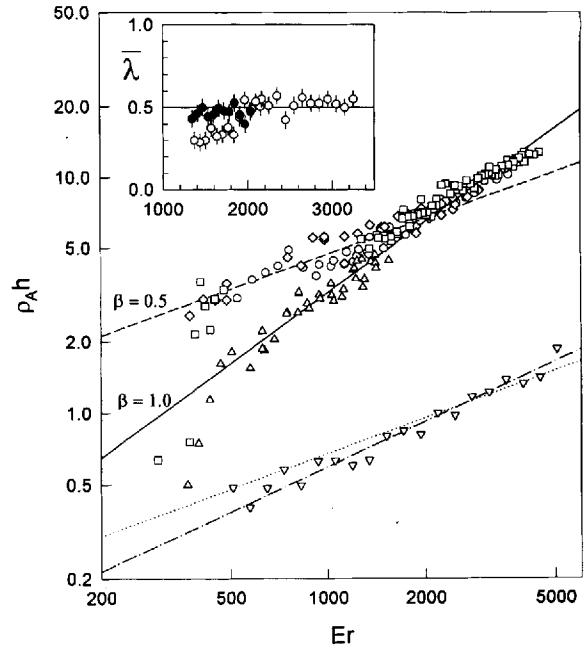

Figure 10. Dimensionless disclination density versus Er for three sample thicknesses $h=250$ (△), 300 (◇), 350 (○), and 400 (□) μm. The solid line represents a best fit of the data (except 250 μm) with the exponent fixed at 0·5 while the single dashed line (- - -) is the best fit with the exponent fixed at 1·0. Also shown are 5CB data (inverted triangles) in the $\tilde{r}$-independent limit ($\tilde{r}=117$) for comparison, with fits in which β is fixed at 0·5 (- - - -) and β is varied (— - —), the latter yielding $\beta=0{\cdot}635$. The inset figure shows the dependence of the disclination profile width, $\bar{\lambda}$ (the average thickness of the disclination-containing slab) on Er for 8CB with $h=400$ (○) and 250 (●) μm.

the power law, $\rho_A h \propto Er^{\beta}$ with a value of $\beta=0{\cdot}5$ for $Er<2000$ and a larger value $\beta\approx1{\cdot}0$ for $Er>2000$. For the *smallest* sample thickness, 250 μm, however, $\beta\approx1{\cdot}0$ for the full range of Er investigated. Consistent with this observation, however, is the dependence of the width of the disclination density distribution, λ, on Er. The inset of figure 10 is a plot of the scaled width of the distribution of disclinations, $\bar{\lambda}=\lambda/h$, as a function of Er for 8CB samples of thickness 400 (○) and 250 (●) μm. We find that coincident with the cross-over from $\beta=0{\cdot}5$ to $\beta=1{\cdot}0$ for the 400 μm sample is the occurrence of saturation of the distribution width at a value $\bar{\lambda}\approx0{\cdot}5$. The distribution width $\bar{\lambda}$ for the 250 μm sample is equal to this value, 0·5, even when Er is below the cross-over value $Er=2000$ found for the other thicknesses; see inset of figure 10. Thus, the persistence of the power-law exponent $\beta=1{\cdot}0$ even at low Er for the 250 μm sample is matched by a corresponding persistence of a saturation value of $\bar{\lambda}=0{\cdot}5$ at these low values of Er. This consistent, yet puzzling, behaviour of the 250 μm sample is unexplained.

4. Discussion

Under a flow gradient, such as the shearing flow studied here, a scaling law for the density of disclinations has been inferred from scaling theory and rheological measurements [16]:

$$\frac{dL}{dt}=k_1\dot{\gamma}L-k_2L^2 \tag{1}$$

where L is the length of disclinations per unit *volume*, $\dot{\gamma}$ is the shearing rate, and k_1 and k_2 are temperature-dependent coefficients. While the no-flow prediction of equation (1), $L\sim t^{-1}$, has been confirmed by Chuang *et al.* [17], our experiments provide the first opportunity to confirm the steady-state prediction of equation (1). To compare our results with equation (1), however, we need to express the experimental observable, ρ_A, in terms of the disclination length per unit volume, L. At steady state, equation (1) predicts [16] the relation,

$$L=(k_1/k_2)\dot{\gamma}=\kappa\frac{\gamma_1}{K_3}\dot{\gamma}. \tag{2}$$

We can define L through the relation

$$\rho_A=\int_0^h\rho_V(y)\,dy=\bar{\lambda}hL, \tag{3}$$

so that,

$$\rho_A h = \kappa\bar{\lambda}\frac{\gamma_1}{K_3}\dot{\gamma}h^2 \propto Er^{1.0}, \quad (4)$$

as confirmed by our data for $\rho_A h > 5$. Similarly, a two-dimensional version of equation (1) in which L is the length of disclinations per unit *area*, leads to the steady-state prediction,

$$\rho_A h \propto Er^{0.5}. \quad (5)$$

Our experiments with 8CB obey equation (4), that is, they show *three-dimensional scaling* of the disclination density when $\rho_A h > 5$, and they show *two-dimensional scaling* when $\rho_A h < 5$ and $h \geqslant 300\,\mu m$ (equation (5)).

At low Er, disclinations are localized at the sample mid-plane presumably because of the symmetry of the repulsive image forces from the bounding discs. The forces a typical disclination feels from other disclinations are therefore largely confined to a plane, and a 2D scaling law should describe the density of disclinations, as we in fact observe for $h \geqslant 300\,\mu m$ and $\rho_A h < 5$. As the disclination density is increased with increasing Er, the disclinations pack near the mid-plane until the density becomes large enough that the disclinations begin to pile-up about the mid-plane; see the inset to figure 10. If the disclinations pile-up to an extent equal to or larger than the 'screening length' of the disclination-disclination interaction forces, then the force on a test disclination is rendered isotropic and the 3D scaling is expected. One would expect the cross-over from 2D to 3D scaling to occur at a fixed value of the dimensionless disclination density, $\rho_A h$, roughly equal to the 'screening length' measured in units of the typical distance between disclinations. This dimensionless length appears to be about 5, according to figure 10.

5. Conclusions

In this and the preceding paper, we have made several important qualitative observations directly comparing the director response of flow-aligning (5CB) and tumbling (8CB) nematic liquid crystals in steady shear flow. Some of these obervations suggest mechanisms of disclination creation in both materials. Additionally, we have reported the first direct measurements of disclination density in flowing liquid crystals.

There are significant qualitative differences between 5CB and 8CB in steady shear flow. For 5CB, as the rotation speed (or Er_R) is increased, the director at first stays within the shear plane, except near the centre of the cell. When Er_R reaches ≈ 4100, large numbers of 'thick' and 'thin' disclinations fill the shear cell, beginning near the edge. No bulk nucleation events are observed, although we speculate that the disclinations originate in the boundary layer. 8CB behaves qualitatively different; the director response to shear flow depends on the rate at which the rotation speed (or Er_R) is increased. For the lowest ramping rate, the director leaves the shear plane, following the creation of a 'disclination band', and points radially outward for $Er = 800$, except near the cell edge, where the director returns to the shear plane. Roll cells form for $Er \approx 1000$, and 'thick' disclination lines nucleate frequently from the boundaries between roll cells.

We find that for both materials, plots of the scaled disclination density, $\rho_A h$, versus Er show power law behaviour of the form, $\rho_A h = \alpha Er^{\beta}$. In the case of 5CB, α and β depend on $\tilde{r}$, except for $\tilde{r} > 90$. 8CB, on the other hand, showed no dependence of $\rho_A h$ on $\tilde{r}$. For 5CB, the scaling exponent, β, was found to be 0·635 for $\tilde{r} > 90$, while 8CB showed scaling exponents of 1·0 and 0·5, depending on the sample thickness. Dimensional reasoning indicates that a scaling exponent of 0·5 is consistent with a 2D definition of the disclination density, while a scaling exponent of 1·0 is consistent with a 3D definition. The distribution of disclinations across the gap is influenced by the total force on each disclination which arises from the long-ranged disclination-disclination and disclination-wall interactions. We conclude that, depending on the *dimensionless* disclination density, this total force may be highly anisotropic (spatially), leading to a 2D scaling exponent, or isotropic, leading to a 3D scaling exponent.

References

[1] Mather, P. T., Pearson, D. S., and Larson, R. G., *Liq. Cryst.*

[2] Wahl, J., and Fischer, F., 1973, *Mol. Cryst. liq. Cryst.*, **22**, 359.

[3] Graziano, D. J., and Mackley, M. R., 1984, *Mol. Cryst. liq. Cryst.*, **106**, 103.

[4] Larson, R. G., and Mead, D. W., 1993, *Liq. Cryst.*, **15**, 151.

[5] Cr, S_A, N and I denote crystalline, smectic A, nematic and isotropic phases, respectively.

[6] Bloss, F. D., 1961, *An Introduction to the Methods of Optical Crystallography*, (Holt, Rinehart, and Winston), p. 108–122.

[7] Manneville, P., Dubois-Violette, P., 1976, *J. Phys. (Paris)*, **37**, 285.

[8] Pieranski, P., and Guyon, E., 1974, *Phys. Rev. A*, **9**, 404.

[9] Larson, R. G., 1993, *J. Rheol.*, **37**, 175.

[10] In H_V light scattering, the incident laser beam is polarized in the flow direction and the analyser after the sample is oriented 90° from the flow direction.

[11] Hsiao, B. S., Stein, R., Deutscher, K., and Winter, H. H., 1990, *J. Polym. Sci. B*, **28**, 1571.

[12] Ernst, B., Navard, P., Hashimoto, T., and Takebe, T., 1990, *Macromolecules*, **23**, 1370.

[13] Skarp, K., Carlsson, T., Lagerwall, S. T., and Stebler, B., *Mol. Cryst. liq. Cryst.*, **66**, 199.

[14] Gu,D.-F., Jamieson, A. M., and Wang, S.-Q., 1993, *J. Rheol.*, **37**, 985.

[15] Mather, P. T., Larson, R. G., Gu, D.-F., and Jamieson, A. M., in preparation.

[16] Larson, R. G., and Doi, M., 1991, *J. Rheol.*, **35**, 539.

[17] Chuang, I., Durrer, R., Turok, N., and Yurke, B., 1991, *Science*, **251**, 1336.